Lateral Control of UAVs: trajectory tracking via Higher-Order Sliding Modes

Syed Ussama Ali
Faculty of Electronic Engineering
Mohammad Ali Jinnah University
Islamabad, Pakistan
Email: ussama.ali@gmail.com

M. Zamurad Shah
Faculty of Electronic Engineering
Mohammad Ali Jinnah University
Islamabad, Pakistan
Email:zamurad@ieee.org

Raza Samar
and Aamer Iqbal Bhatti
Faculty of Electronic Engineering
Mohammad Ali Jinnah University
Islamabad, Pakistan
Email: raza.samar@gmail.com
Email: aib@jinnah.edu.pk

***Abstract*—Nonlinear sliding mode approach is developed in this paper for lateral control of UAVs. The enabling guidance and control has achieved good performance with different flight conditions and evasive maneuvers. The proposed strategy can recover from large track errors without effecting the saturation constraints on the control input. The structure of guidance and flight control system is designed in a two loop configuration. The main contribution of this work is the development of new guidance scheme in which inner loop dynamics are also considered during the derivation of outer guidance loop for robust lateral control and never forcing unsuitable commands. HOSM (Higher-Order Sliding Mode) Real Twisting Algorithm is used because of relative degree 2 constraint, which maintains S and $\dot{S} = 0$. The outer loop for guidance uses heading error angle, lateral track error and bank (roll) angle ϕ for the control law and PD controller is used in the inner loop. The designed guidance control system's robustness and performance is verified via computer simulations using high fidelity nonlinear 6-degrees-of-freedom (6-dof) Yak-54 UAV model under different scenarios, with small and large track errors and in the presence of wind disturbances.**

I. Introduction

Unmanned Aerial Vehicles (UAVs) are increasingly being used in civilian and military applications due to relatively low operational cost and reduce risk to life. To the problem of trajectory tracking of UAVs, two strategies are mainly used. In the first strategy, UAV guidance and control is divided in to two loop structure, outer loop for guidance and inner loop for control [1], [2], [3] and [4]. The outer guidance loop generates the desired reference bank (roll) angle on the basis of heading angle and lateral track error. The inner control loop is responsible for generating commands to control surface respective to the required bank angle. In the second strategy, often the two loop structure is replaced by a single integrated loop in which the guidance and control laws are designed together in a single framework [5], [6] and [7]. Mostly the first approach i.e the two loop structure is commonly used for different applications due to its simplicity and availability of elegant/robust design methods for inner loop control. In the past, different approaches have been used for outer guidance loop. In many UAV applications linear proportional PD control [8] has been used. If the desired trajectory path is a straight line, then this simple strategy will provide reasonably good outer loop performance. But in the presence of wind disturbance or during following a curved path performance of PD control degrades. To overcome the drawbacks of PD control a nonlinear approach was suggested in [9], [10] showing improved robustness and performance. But for large track errors the control output of this nonlinear scheme saturates. And no stability and boundedness proof of control input during saturation are given. To enhance the tracking performance, linear proportional and derivative lateral control was improved with some nonlinear modifications in [11]. But the design scheme proposed by [11] gives an informal solution and no stability analysis is given. In literature, several different strategies have been proposed by [12], [13], [14].

Performance of trajectory tracking under heavy uncertain conditions still remains among the main topics of control theory. Sliding Mode Control (SMC) [15] technique turns out to be characterized by high simplicity and robustness and is extensively discussed in [15], [16]. Essentially, SMC utilizes discontinuous control laws to drive the system state trajectory onto a specialized surface, the so called sliding or switching surface, and to keep the system state on this manifold for all the subsequent times [17]. In order to achieve the control objectives, the control input must be designed with sufficient authority to overcome the bounded uncertainties and the disturbances acting on the system. However, in spite of the claimed robustness properties, the implementation of sliding mode control algorithm presents a major drawback: the so called chattering effect. The two main criticisms to sliding modes control technique are chattering and the need for continuous control, and these shortcomings are much more obvious when considering mechanical systems. Therefore SMC gave birth to many variants which includes high gain control with saturation [16], multi gain sliding mode, transformation of discontinuities into continuous approximation [17], dynamic sliding mode control [17], [16], the sliding sector method [18] and smoothness from asymptotic state observers [19]. However, higher order sliding mode specially the real twisting algorithm [20] approach is more convenient. Sigmoid functions and saturations are used as filters for the output of a discontinuous signal in order to obtain a continuous one that is realizable by mechanical hardware.

In this work, the strategy adopted is the two loop structure in which the UAV guidance and control problem is divided into two loops. The outer loop for guidance and inner loop for control. It is assumed that the desired reference roll angle can be tracked by already designed inner control law with

978-1-4673-5769-2/13/$31.00 ©2013 IEEE

minimum overshoot. For robust tracking a new sliding mode based approach was proposed in our previous work [2] for outer guidance loop. The outer guidance loop is responsible for generating the desired/reference roll angle on the basis of current heading error angle and lateral track error. In order to meet the robustness and high performance constraints for small track error and a bounded heading error angle in the case of large track error, a new state was taken into account in addition to a nonlinear sliding surface proposed in [2]. By doing so the closed loop dynamics of the system for roll angle ϕ is also incorporated in the design scheme. Real twisting algorithm is used to generate ϕ_{ref}, its stability analysis and boundedness proof is also given. Also the proposed scheme is implemented in non-linear 6-dof simulation and simulation results of different cases are shown here, that validate the robustness of this proposed scheme.

The structure of the paper is as follows: The analytical model of the problem by providing the variables and equations that describe the behavior of guidance of UAV and its nonlinear dynamics is presented in Section II. Section III, presents the proposed guidance law on the basis of HOSM (Higher Order Sliding Mode) Real Twisting Algorithm. In Section IV, stability analysis and boundedness of the feedback guidance loop is given to validate the control methodology for achieving tight control of lateral dynamics. Section V shows some simulation results followed by conclusion, references and appendix.

II. PROBLEM STATMENT AND FORMULATION

Notation of different variables used in this paper is same as used in [8], [11] and [2]. Here, y lateral (or cross-track) displacement of the vehicle, $\psi_{_R}$: angle of the line $WP1$-$WP2$ with respect to north (reference/desired heading angle) and $\psi_{_G}$: heading angle of the UAV w.r.t north (Velocity heading). $\psi_{_E} = \psi_{_G} - \psi_{_R}$. Note that magnitude of $\psi_{_E}$ should be less than 90 degrees.

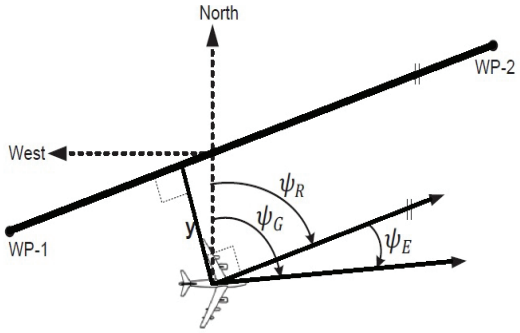

Fig. 1. Definition of Cross track error y, ψ_G, ψ_R and ψ_E

Large cross-track deviations can in practice arise due to many reasons. Large lateral disturbances, such as strong persistent winds, Change of mission during flight, Loss of the GPS signal. The main task of the guidance law is to generate a smooth bounded ϕ_r to keep the lateral cross-track error y small in the presence of disturbances. In case a cross-track error develops, it should be smoothly brought to zero, without excessive overshoot, while maintaining the basic flight direction $WP1 \rightarrow WP2$. The overall guidance and control system must maintain stability during flight.

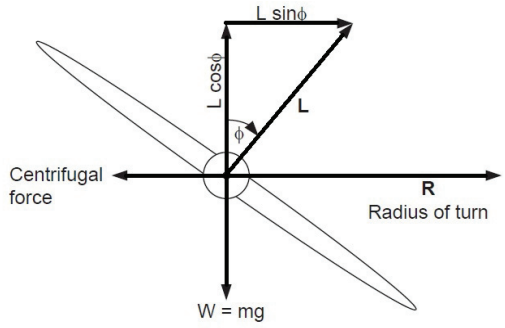

Fig. 2. Lift Components during turn

Aerial vehicles use a component of the aerodynamic lift to generate lateral accelerations to correct lateral (cross-track) errors. $L\cos\phi = mg, L\sin\phi = \frac{mV^2}{R}, \tan\phi = \frac{V^2}{Rg}$. Using $V = R\dot{\psi}_{_G}$, $\psi_{_E} = \psi_{_G} - \psi_{_R}$, and $\dot{\psi}_{_R} \approx 0$.

$$\dot{y} = V\sin\psi_E \tag{1}$$

$$\dot{\psi_E} = \frac{g}{V}\tan\phi \tag{2}$$

We shall make the following simplifying assumptions during our treatment of the guidance problem. The control law for the inner loop is available; the inner loop controller can be designed using well established techniques, such as robust linear control design methods [21], [22]. But instead of assuming that the inner loop dynamics from ϕ_{ref} to ϕ is fast enough and its dynamics can be ignored [2], here we consider the inner dynamics during outer guidance loop design. For simplicity, inner loop dynamics can be approximated by a first order transfer function.

$$\frac{\phi}{\phi_{ref}} = \frac{1}{\tau s + 1} \tag{3}$$

$$\dot{\phi} = \frac{1}{\tau}(\phi_{ref} - \phi) \tag{4}$$

y, $\psi_{_E}$ and ϕ are the state variables, and ϕ_{ref} is the control signal that the guidance loop generates for track following.

III. LATERAL CONTROL SCHEME

The control law should be designed, to attract the system state trajectories from any arbitrary initial condition towards the sliding manifold so called the reaching phase and then slides along the manifold, the sliding phase [23]. The dynamics of the system while in sliding is insensitive to model uncertainties and disturbances [15], [16] and [20]. The attractivity of the sliding surface can be expressed by the condition (also known as reachability condition) [17]. For good performance in case of both small and large track errors, and to keep the magnitude of ψ_E less than $\frac{\pi}{2}$, a nonlinear sliding surface is proposed in [2]:

$$S = \psi_E + \alpha\arctan(\beta y) = 0, \tag{5}$$

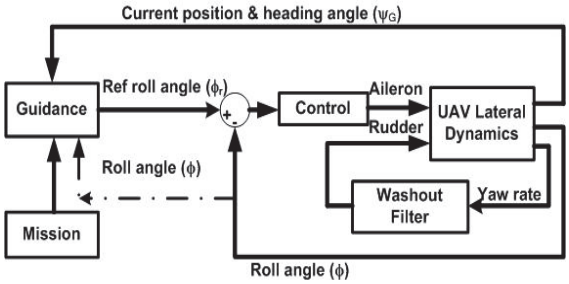

Fig. 3. Block Diagram of Guidance and Control Methodology

where $\alpha, \beta \in \Re$, and the sliding surface stability requires $\alpha\beta > 0$. We need $|\alpha| < 1$ in order to ensure $|\psi_E| < \frac{\pi}{2}$. Here, we have used the same sliding surface with different methodology by using ϕ in the guidance block as can be seen from Fig. 3 for generating ϕ_{ref}.

$$\dot{S} = \dot{\psi_E} + \frac{\alpha\beta}{1+\beta^2 y^2}\dot{y} \tag{6}$$

Along the system state derivatives

$$\dot{S} = \frac{g}{V}\tan\phi + \frac{\alpha\beta}{1+\beta^2 y^2}(V\sin\psi_E) \tag{7}$$

In our previous work, inner dynamics was ignored with the assumption that $\phi_{ref} \approx \phi$ and hence the relative degree of system was 1 in that case but here relative degree of system is > 1 and the control law is designed using the Higher Order Sliding Mode Real Twisting controller.

$$\dot{S} = \frac{g}{V}\tan\phi + \frac{\alpha\beta}{1+\beta^2 y^2}V\sin\psi_E \tag{8}$$

$$\ddot{S} = \frac{g}{V}\frac{d}{dt}(\tan\phi) + \frac{d}{dt}\frac{V\alpha\beta\sin\psi_E}{1+\beta^2 y^2} \tag{9}$$

With the new state equation i.e $\dot{\phi}$, for the control input ϕ_{ref} to appear, the 2^{nd} derivative of the sliding surface (5) render the form

$$\begin{aligned}\ddot{S} =& \frac{g}{V}\sec^2\phi\frac{1}{\tau}(\phi_{ref}-\phi) + \frac{g\alpha\beta\tan\phi\cos\psi_E}{(1+\beta^2y^2)^2} \\ &+ \frac{g\alpha\beta^3y^2\tan\phi\cos\psi_E}{(1+\beta^2y^2)^2} - \frac{2V^2\alpha\beta^3y\sin^2\psi_E}{(1+\beta^2y^2)^2}\end{aligned} \tag{10}$$

1) Real Twisting Algorithm: To cope up with the nonlinearities, sliding mode control uses very high frequency control input to stabilize the plant [17]. The capacity to divide complex higher order problems into relatively smaller tasks of simpler scope and the inherent properties are the main benefits of sliding mode control [17].

The design methodology of HOSM (Higher-Order Sliding Mode) is similar to SMC (Sliding Mode Control). But in HOSM, the constraints $s = \dot{s} = 0$ must be fulfilled i.e the higher order derivatives of sliding manifold must be equal to zero. So as to compensate for chattering a new control algorithm was developed [20] in which imperative properties of sliding mode control are preserved and real discontinuities are avoided. "Real- Twisting" 2-sliding controller [20], [17] can be used for controlling the systems with relative degree two. The relative degree is defined as the no of derivatives of sliding variable, for the control input to appear. As in our case, the ϕ_{ref} appears in $\ddot{S}$ the second derivative of the sliding variable, relative degree is 2. The continuous control law u comprises of two terms and the state trajectories are described by twisting around the origin [17]. The first term in control law is a discontinuous term on S, while the other is a discontinuous function of $\dot{S}$. A Real twisting controller appears in the following form

$$\ddot{S} = a(t) + b(t)u \tag{11}$$

Where $|a(t,x)| \leq C$ and $0 \leq k_m \leq b(t,x) \leq k_M$ [24]. Then the control law appears as

$$u = -r_1 Sign(S) - r_2 Sign(\dot{S}) \tag{12}$$

Now using the (12) with our system dynamics. The expression for ϕ_{ref} using the control law in (12) with S as in (5) and $\dot{S}$ as in (6) becomes

$$\begin{aligned}\phi_{ref} =& -r_1 Sign(\psi_E + \alpha\arctan(\beta y)) \\ &- r_2 Sign(\frac{g}{V}\tan\phi + \frac{\alpha\beta V\sin\psi_E}{1+\beta^2y^2})\end{aligned} \tag{13}$$

$$\begin{aligned}\ddot{S} =& \frac{g\phi_{ref}}{V\tau}\sec^2 - \frac{g\phi}{V\tau}\sec^2 + \frac{g\alpha\beta\cos\psi_E\tan\phi}{(1+\beta^2y^2)^2} \\ &+ \frac{g\alpha\beta^3y^2\cos\psi_E\tan\phi}{(1+\beta^2y^2)^2} - \frac{2V^2\alpha\beta^3y\sin^2\psi_E}{(1+\beta^2y^2)^2}\end{aligned} \tag{14}$$

Since ϕ_{ref} is our desired control input therefore

$$b(t,x) = \frac{g\sec^2\phi}{V\tau} \tag{15}$$

$$\begin{aligned}a(t,x) =& -\frac{g\phi\sec^2\phi}{V\tau} + \frac{g\alpha\beta\cos\psi_E\tan\phi}{(1+\beta^2y^2)^2} \\ &+ \frac{g\alpha\beta^3y^2\cos\psi_E\tan\phi}{(1+\beta^2y^2)^2} - \frac{2V2\alpha\beta^3y\sin^2\psi_E}{(1+\beta^2y^2)^2}\end{aligned} \tag{16}$$

IV. STABILITY ANALYSIS AND BOUNDEDNESS OF CONTROL EFFORT

As the roll angle of aerial vehicle increases, the aerodynamic lift required to balance the weight decreases. Inner control loop actuates the control surface to follow the desired/reference roll angle ϕ_{ref} generated by outer guidance loop. So the reference roll angle ϕ_{ref} must be bounded by some limit ϕ_{max}. In this section we derive the conditions for keeping $|\phi_{ref}| \leq \phi_{max}$ and $\phi_{max} = \frac{\pi}{4}$ during the reaching and sliding motion on the surface. For the controller, four inequalities must be satisfied which includes

$$r_1 > r_2 > 0 \tag{17}$$

$$r_1 + r_2 \leq 45 \tag{18}$$

$$k_m(r_1+r_2) - C > k_M(r_1-r_2) + C \tag{19}$$

$$k_m(r_1+r_2) > C \tag{20}$$

The expression in (17), (19) and (20) proves the stability and existence of $2-$sliding mode [24]. While the Eq.(18) is induced by our design strategy that the $|\phi_{ref}| \leq \frac{\pi}{4}$.

$$b(t,x) = \frac{g\sec^2\phi}{V\tau} \tag{21}$$

For K_M i.e the maximum bound on (21)

$$K_M = \frac{g}{V_{min}\tau}\frac{1}{\cos^2\phi_{min}} \tag{22}$$

For K_m i.e the minimum bound on on (21)

$$K_m = \frac{g}{V_{max}\tau}\frac{1}{\cos^2\phi_{max}} \tag{23}$$

$$|a(t,x)| \leq C \tag{24}$$

Therefore for calculating the maximum bound C

$$|a(t,x)| = |a_1(t,x) + a_2(t,x) + a_3(t,x) + a_4(t,x)| \tag{25}$$

$$a_1 = -\frac{g\phi\sec^2\phi}{V\tau} \tag{26}$$

The absolute maximum value of $|a_1|$ is 1.710 which occurs at $V_{min} = 30$ and $\tau = 0.3$. The value of α and β is chosen as 0.75 and 0.005 respectively.

$$a_2 = \frac{g\alpha\beta\cos\psi_E\tan\phi}{(1+\beta^2y^2)^2} \tag{27}$$

$$a_3 = \frac{g\alpha\beta^3y^2\cos\psi_E\tan\phi}{(1+\beta^2y^2)^2} \tag{28}$$

The absolute maximum value of $|a_2|$ and $|a_3|$ is 0.03675 and 0.00918 respectively, which depends on different variables ψ_E, ϕ and y. It occurs when $\cos\psi_E$ and $tan\phi$ are maximized to 1 and cross track error is zero for $|a_2|$ and cross track error is 200m for $|a_3|$.

$$a_4 = -\frac{2V^2\alpha\beta^3y\sin^2\psi_E}{(1+\beta^2y^2)^2} \tag{29}$$

The absolute maximum value of $|a_4|$ is 0.0164, which happens when the term V is 37. The term $\sin^2\psi_E$ is maximum when ψ_E is equal to -90^o or 90^o, cross track error is 110m.

$$|a_1(t,x) + a_2(t,x) + a_3(t,x) + a_4(t,x)| \leq C \tag{30}$$

The control input bounds i.e K_M and K_m are 2.1777 and 0.8828 respectively. With r_1 and r_2 chosen as 30 and 15 respectively, all the inequalities given above are satisfied. Then the controller in (12) provides for the appearance of a 2-sliding mode i.e $s = \dot{s} = 0$ attracting the trajectories in finite time.

V. SIMULATION RESULTS

The proposed strategy is implemented in simulation with $sign(s) = \frac{s}{|s|+\epsilon}$ (the approximation of signum function). Simulation results are shown here for small cross track error, large cross track error with no wind and large cross track error with (10m/s North) wind. To see the robustness of this proposed algorithm, simulations are performed in the presence of disturbance (wind). Maximum steady state error in cross range in the case of small track error is 2 meters, for large cross track error with no wind is 0.6 meters and for large cross track error with (10m/s North) wind is 1.2 meters respectively. Simulation results also validate that there is no control effort saturation during motion on sliding surface. Problem of chattering in standard sliding mode technique is settled using real twisting HOSM and by smoothing the control input using boundary layer during implementation of this proposed algorithm.

A. Small Cross Track Error

In Fig. 4, simulation results with proposed guidance logic are shown for an initial cross track error of 400m in case of straight path following. First subplot of Fig. 4 shows the UAV phase portrait and the sliding surface. Cross track error y and the heading error ψ_E vs time are shown in second and third subplot respectively. Fourth subplot of Fig. 4 sows the reference roll angle generated by the outer guidance logic. Cross track error reduced from 400m to 2m in 35sec.

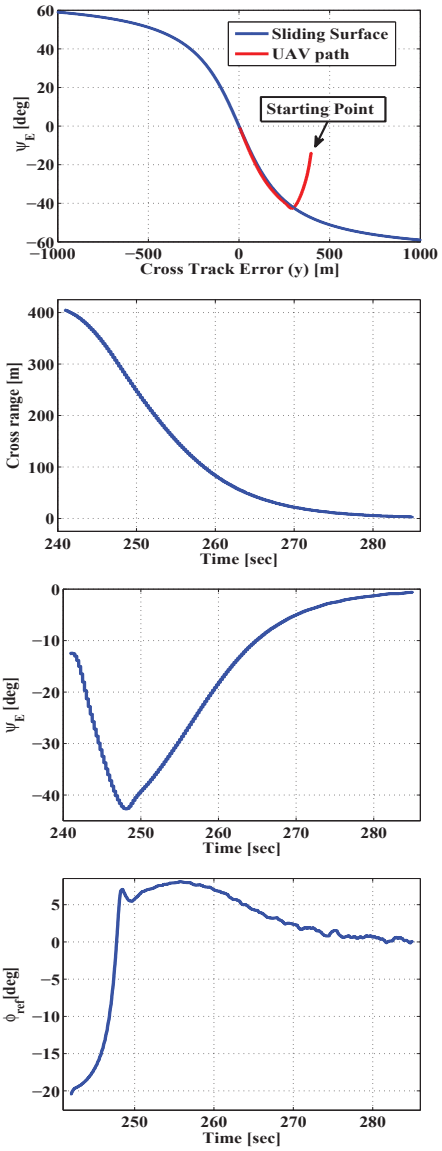

Fig. 4. Performance for 400m cross track error (No wind)

B. Large Cross Track Error

In Fig. 5, Fig. 6 and Fig. 7, simulation results with proposed guidance logic are shown for an initial cross track error of 1000m in case of straight path following. Fig. 5 shows the UAV phase portrait and the sliding surface, cross track error y is also shown in the same plot. Reference roll angle ϕ_{ref} and the corresponding inner loop control effort δ_a is shown in Fig. 6,

it is evident that the control effort is in our desired limits. The HOSM real twisting controller derives the trajectories of S and $\dot{S}$ to zero which can be observed in Fig. 7. Cross track error reduced from 1000m to 0.6m in 57sec.

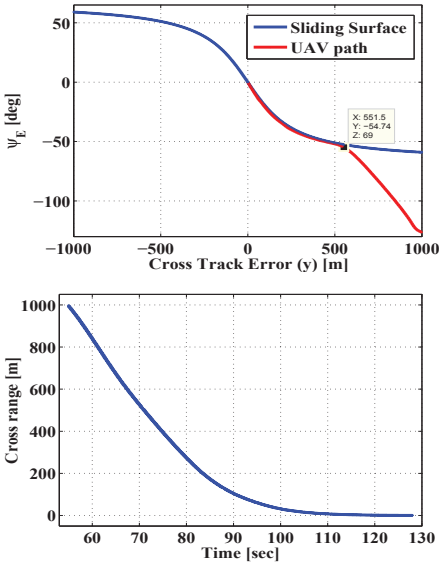

Fig. 5. Performance for 1000m cross track error (No wind)

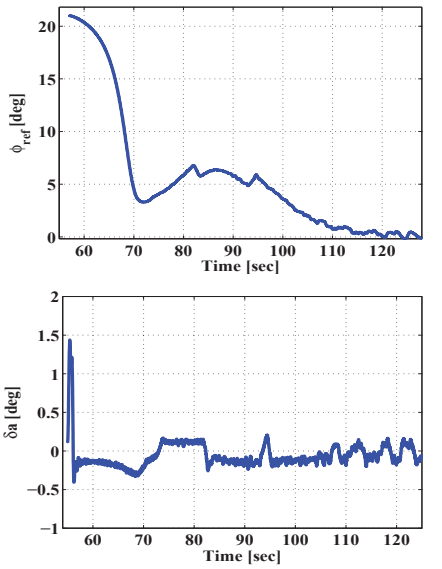

Fig. 6. Performance for 1000m cross track error (No wind)

The HOSM real twisting controller (12) provides the appearance of a 2-sliding mode, the state trajectories are attracted in finite time i.e $s = \dot{s} = 0$ as can be seen from Fig. 7

C. Large Cross Track Error with 10m/s North Wind

Further, the robustness of the HOSM controller in the presence of disturbance is validated. Simulation results for 1000m track error in the presence of 10m/s side wind are

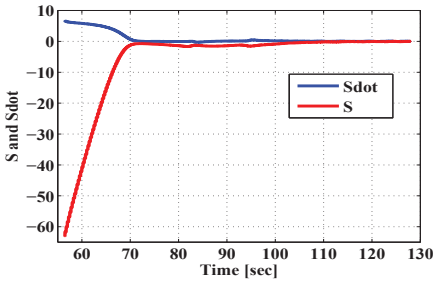

Fig. 7. Performance for 1000m cross track error (No wind)

shown in Fig. 8. As evident from Fig. 8, there is no overshoot in cross track error and magnitude of steady state track error is less than 2.5 meters. Fig. 8 also validate that during motion on sliding surface maximum control effort is with in our desired limit.

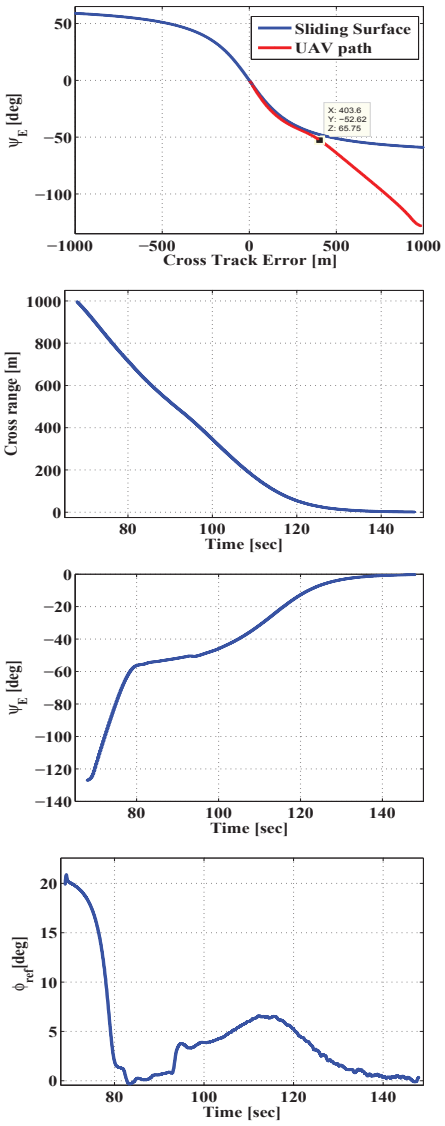

Fig. 8. Performance for 1000m cross track error (10m/s North wind)

VI. Conclusion

A robust guidance and control system for UAVs is introduced in this paper. Nonlinear sliding surface based on higher order sliding mode control theory is used in this new scheme. Due to the limitations of performance in the case of small track error and to keep for whole flight envelope, a non-linear sliding surface that can meet both these limitations is proposed in [2] and its stability analysis using lyapunov function is also presented. But inner loop dynamics from ϕ_{ref} to ϕ was ignored in derivation of outer guidance logic in [2]. Therefore same sliding surface is used in this paper with different set of framework when considering dynamics from ϕ_{ref} to ϕ. Problem of chattering in standard sliding mode technique is settled by smoothing the control input by using higher order sliding mode (HOSM) i.e Real Twisting Algorithm. Performance of numerical simulations for different cases, along with the stability analysis is given in this work. Using simulations, it was shown that with the new method, vehicle will follow a desired trajectory better than the traditional techniques. The reasons for the better performance can be explained as, the angle ϕ_{ref} generated by the guidance logic serves two purposes. First, it provides suitable roll angles against small deviations on the track error. Secondly, it provides a heading correction.

Acknowledgment

The authors would like to thank CASPR (Control And Signal Processing Research Group).

References

[1] R. Samar, S. Ahmed, and M. Nzar, "Lateral guidance & control design for an unmanned aerial vehicle," in 17^{th} *IFAC World Congress*, Seoul, 2008.

[2] M. Z. Shah, R. Samar, and A. I. Bhatti, "Lateral control for UAVs using sliding mode technique," in 18^{th} *IFAC World Congress*, Milano, Italy, 2011.

[3] M. Niculescu, "Lateral track control law for Aerosonde UAV," in *39th AIAA Aerospace Sciences Meeting and Exhibit*, Reno, NV, 8-11 January 2001.

[4] R. Rysdyk, "Unmanned aerial vehicle path following for target observation in wind," *Journal of Guidance, Navigation, and Control*, vol. 29, no. 5, pp. 1092–1100, 2006.

[5] I. Kaminer, A. Pascoal, E. Hallberg, and C. Silvestre, "Trajectory tracking for autonomous vehicles: An integrated approach to guidance and control," *AIAA journal of Guidance, Control, and Dynamics*, vol. 21, no. 1, pp. 29–38, 1998.

[6] T. Yamasaki1 and S. N. Balakrishnan, "Preliminary assessment of flying and handling qualities of mini-UAVs," *Journal of Aerospace Engineering*, vol. 224, no. 10, pp. 1057–1067, 2010.

[7] J. Yu, Q. Xu, and Y. Zhi, "A TSM control scheme of integrated guidance/autopilot design for UAV," in *3rd International Conference on Computer Research and Development (ICCRD)*, Shanghai, China, 11-13 March 2011.

[8] G. M. Siouris, *Missile Guidance and Control Systems*. Springer-verlag, USA, 2004.

[9] S. Park, J. Deyst, and J. How, "A new nonlinear guidance logic for trajectory tracking," in *AIAA Guidance, Navigation, and Control Conference and Exhibit*, Providence, Rhode Island, 16-19 August 2004.

[10] J. Deyst, J. How, and S. Park, "Lyapunov stability of a nonlinear guidance law for UAVs," in *AIAA Atmospheric Flight Mechanics Conference and Exhibit*, San Francisco, CA, 15-18 August 2005.

[11] R. Samar, S. Ahmed, and M. F. Aftab, "Lateral control with improved performance for UAVs," in 17^{th} *IFAC Symposium on Automatic Control in Aerospace*, Toulouse, France, 2007.

[12] D. R. Nelson, D. Blake, B. Timothy, W. Mclain, and R. W. Beard, "Vector field path following for small unmanned air vehicles," in *IEEE Transactions on Control Systems Technology*, 2006, pp. 5788–5794.

[13] N. Regina and M. Zanzi, "UAV guidance law for ground-based target trajectory tracking and loitering," in *Proceedings of the IEEE Aerospace Conference*, March 2011.

[14] Y. Shtessel, I. Shkolnikov, and A. Levant, "Guidance and control of missile interceptor using second-order sliding modes," *Aerospace and Electronic Systems, IEEE Transactions on*, vol. 45, no. 1, pp. 110 –124, jan. 2009.

[15] Y.-W. Kim, G. Rizzoni, and V. Utkin, "Automotive engine diagnosis and control via nonlinear estimation," *Control Systems Magazine, IEEE*, vol. 18, no. 5, pp. 84 –99, oct 1998.

[16] C. Edwards and S. K. Spurgeon, *Sliding Mode Control: Theory and Applications*. Taylor and Francis, 1998.

[17] W. Perruquetti and J. P. Barbot, *Sliding Mode Control in Engineering*. New York - Basel: Marcel Dekker Inc., 2002.

[18] K. Furuta and Y. Pan, "Variable structure control with sliding sector," *Automatica*, vol. 36, no. 2, pp. 211 – 228, 2000. [Online]. Available: http://www.sciencedirect.com/science/article/pii/S0005109899001168

[19] Y. Shtessel, I. Shkolnikov, and M. Brown, "An asymptotic second-order smooth sliding mode control," *Asian Journal of Control*, vol. 4, no. 5, pp. 959–967, 2003.

[20] A. Levant, "Sliding order and sliding accuracy in sliding mode control," *International Journal of Control*, vol. 58, no. 6, pp. 1247–1263, 1993.

[21] D. McFarlane and K. Glover, *Robust Controller Design Using Normalized Coprime Factor Plant Descriptions*, ser. Lecture Notes in Control and Information Sciences. Berlin: Springer-Verlag, 1990, vol. 138.

[22] S. Skogestad and I. Postlethwaite, *Multivariable Feedback Control: Analysis and Design*, 2nd ed. John Wiley & Sons, INC., October 2005.

[23] B. Bandyopadhyay, F. Deepak, and K.-S. Kim, *Sliding Mode Control Using Novel Sliding Surfaces*. Springer-Verlag Berlin Heidelberg: Springer, 2009.

[24] I. Sohail, "Robust smooth model-free control methodologies for industrial applications," Ph.D. dissertation, Department of Electronic Engineering, Mohammad Ali Jinnah University, 2011.